Published in final edited form as:
J Neurosci Methods. 2014 May 30; 229: 44–52. doi:10.1016/j.jneumeth.2014.04.001.

A novel technique for morphometric quantification of subarachnoid hemorrhage-induced microglia activation

Benjamin A. Plog, B.A.[a,b,c], **Katherine M. Moll, B.A.**[a,b], **Hongyi Kang, B.A.**[b], **Jeffrey J. Iliff, Ph.D.**[b,a], **Maiken Nedergaard, D.M.Sc., Ph.D.**[b], and **G. Edward Vates, M.D., Ph.D.**[b]

Katherine M. Moll: Katherine_Moll@urmc.rochester.edu; Hongyi Kang: Hongy_Kang@urmc.rochester.edu; Jeffrey J. Iliff: iliffj@ohsu.edu; Maiken Nedergaard: Maiken_Nedergaard@urmc.rochester.edu; G. Edward Vates: Edward_Vates@urmc.rochester.edu

[a]University of Rochester School of Medicine and Dentistry, Rochester, NY, USA

[b]Department of Neurosurgery, Center for Translation Neuromedicine, University of Rochester Medical Center, Rochester, NY, USA

[c]Department of Pathology, University of Rochester Medical Center, Rochester, NY, USA

Abstract

Background—Subarachnoid hemorrhage (SAH) is a neurologic catastrophe and poor outcome is typically attributed to vasospasm; however, there is also evidence that SAH causes a pro-inflammatory state and these two phenomena may be interrelated. SAH causes activation of microglia, but the time course and degree of microglial activation after SAH and its link to poor patient outcome and vasospasm remains unknown.

New Method—Transgenic mice expressing eGFP under the control of the CX3CR1 locus, in which microglia are endogenously fluorescent, were randomly assigned to control or SAH groups. Immunohistochemistry for CD-68 and CD-31 was performed at different time points after SAH. Using confocal microscopy and MatLab software, we have developed a novel technique to detect and quantify the stages of microglial activation and return to quiescence using an automated computerized morphometric analysis.

Results—We detected a statistically significant decrease in microglial process complexity 2 and 7 days following SAH. In addition, we detected a statistically significant increase in microglial domain volume 1 day following SAH; however, microglial domain volume returned to baseline by 2 days.

Corresponding Author: Benjamin A. Plog, 601 Elmwood Avenue, Box 80, Rochester, NY 14642, Benjamin_Plog@urmc.rochester.edu, (518) 928-7898.

Previous Presentations of Work: Portions of this work were presented as proceedings at the 79th American Association of Neurological Surgeons Annual Meeting, Denver, CO, USA, April 13, 2011.

6. Disclosure

The authors report no conflict of interest including any financial, personal, or other relationships with other people or organizations concerning the materials or methods used in this study or the findings specified in this paper.

Comparison with Existing Method—Most techniques for microglia assessment are qualitative, not quantitative, and are therefore inadequate to address the effects of anti-inflammatory drug treatment or other therapies after SAH.

Conclusions—Using novel image analysis techniques we were able to reproducibly quantify activation of microglia following SAH, which will improve our ability to study the biology of microglial activation, and may ultimately improve management of disease progression and response to therapies directed at microglial activation.

Keywords

subarachnoid hemorrhage; microglia; morphology; inflammation; mouse

1. Introduction

Aneurysmal subarachnoid hemorrhage (SAH) is a devastating neurologic event that causes poor neurologic outcomes in patients for a variety of reasons (Macdonald et al., 2007; Rosengart et al., 2007; Suarez et al., 2006; Vergouwen et al., 2011). Cerebral vasospasm is a common consequence of SAH, and can cause cerebral ischemia and infarction (Crowley et al., 2011; Macdonald et al., 2007; Vergouwen et al., 2011). Patients with vasospasm, however, do not necessarily develop strokes, and many patients with ischemia-related neurologic deficits do not demonstrate vasospasm (Rosengart et al., 2007; Suarez et al., 2006; Vergouwen et al., 2011). This has lead to a reinvigorated search for other mediators of neurologic injury after SAH (Cahill and Zhang, 2009; Hansen-Schwartz et al., 2007; Macdonald et al., 2007; Pluta et al., 2009). Recently, the literature has focused on the impact of early brain injury (EBI), cortical spreading depression, and global ischemia on patient morbidity and mortality in the wake of SAH (Dreier, 2011; Dreier et al., 2006; Ostrowski et al., 2006; Sehba and Bederson, 2006; Sehba et al., 2011), but much of the pathogenesis of this disease still remains to be understood. Currently, there is increased interest in the investigation of changes involving the microcirculation, specifically changes in capillary blood flow (Dóczi, 2001; Friedrich et al., 2010; KoŸniewska et al., 2006; Perkins et al., 2002; Sehba and Friedrich, 2011; Sehba et al., 2005; Sehba et al., 2004), changes in the blood brain barrier (Hansen-Schwartz et al., 2007; Macdonald et al., 2007; Ostrowski et al., 2006; Sehba et al., 2004; Sehba et al., 2011), and the inflammatory processes that occur after SAH in a mouse model of SAH (Dumont et al., 2003; Frijns and Kappelle, 2002; Sercombe et al., 2002; Simi et al., 2007).

SAH can be considered a pro-inflammatory state due to the profound consequences of extravasation of blood into the subarachnoid space (Dreier et al., 2000). Previous studies have been able to demonstrate an array of SAH-induced inflammatory processes including: the evolution of pro-inflammatory cytokines such as IL-1, TNF-alpha, and IL-6; the activation of lipoxygenases, cyclooxygenases, and nitric oxide synthases; the release of sensory nerve neuropeptides and the ensuing neurogenic inflammation; blood brain barrier deterioration resulting from the release of neurotransmitters such as histamine, serotonin, and bradykinin; hemoglobin release from lysed erythrocytes and the impact on endothelial and smooth muscle physiology; and even endothelin molecules as potential inflammatory mediators or mitigators (Dumont et al., 2003; Sercombe et al., 2002). As microglia are the

resident inflammatory cells in the brain (Graeber, 2010), it seems reasonable that there would be a dynamic interplay between microglia and these aforementioned processes in the pathophysiology of SAH. There is some evidence that SAH can cause activation of microglia (Liu et al., 2011; Murakami et al., 2011; Ransohoff and Cardona, 2010), but the time course and degree of microglial activation after SAH remains poorly described, in part because the quantification of microglial activation has depended on immunohistochemical techniques that are prone of artifacts. In order to better study what role microglia play in SAH we need improved techniques for both the detection and quantification of their activation.

In the current study, we hypothesize that 1) microglia are activated in a commonly used mouse model of SAH, 2) using a transgenic mouse line, in which microglia are endogenously fluorescent, we can detect microglial activation using novel computerized morphometric analysis, and 3) stages of microglial activation and return to quiescence can be detected and statistically quantified.

2. Experimental Procedures

2.1 Mouse Model

Cx3cr1-eGFP (+/−); enhanced green fluorescent protein (eGFP) is expressed under the endogenous Cx3cr1 promoter of C57BL/6N mice (Charles River Laboratories International). The CX3C chemokine receptor 1 (Cx3cr1; fractalkine receptor) promoter is constitutively turned on in microglia, and thus allows selective imaging of this cell population when eGFP is placed under this promoter's control (Jung et al., 2000; Prinz and Priller, 2010).

2.2 Cisterna Magna Autologous Blood Injection Model of Subarachnoid Hemorrhage

All experimental protocols were approved by the University Committee on Animal Resources of the University of Rochester Medical Center (protocol # 2006-140). Mice (8–12 weeks, 20–25 g) were nil per os (NPO) for 12 hours preceding any experimental intervention to eliminate any confounding effects of varying blood glucose levels on microglial reactivity. During this 12-hour period all oral food was discontinued, however, water intake was not restricted. Mice were then randomized into one of four experimental conditions: control, 1 day, 2 day, or 7 day SAH (fig. 1). Mice were anesthetized with a mixture of ketamine (60 mg/kg, ip) and xylazine (10 mg/kg, ip) and had femoral artery catheterization. For the cisterna magna autologous blood injection model of SAH, 60 μL of autologous blood was withdrawn from the femoral artery before injection into the cisterna magna. An equivalent volume of lactated ringer's was replaced intraperitoneally after blood removal. The mice were then placed in the prone position with the head flexed below horizontal by approximately 30°. With the aid of a Zeiss operating microscope, the posterior scalp was incised in the midline and the skull exposed at the craniocervical junction. The occipital muscles were carefully dissected off the occipital bone and retracted inferolaterally. The atlanto-occipital membrane was exposed and the cisterna magna cannulated with a 30-gauge needle angled 45° caudally and through which the autologous blood was injected over a period of 5 minutes in order to prevent the egress of blood through

the cannulation site or sudden apnea within the experimental animal. Animals were then immediately placed in a head-down position for 10 minutes to facilitate the diffusion of injected blood in the basal cisterns. The needle was removed and wound closed in a standard fashion; similarly the femoral artery catheter was removed and the groin wound closed. After SAH surgery, animals recovered while being observed for health and pain in a private cage where food and water was available. Control mice experience the above protocol with the exception of a 0.01M phosphate-buffered saline (PBS) (pH 7.4, Sigma-Aldrich) injection instead of a blood injection to the cisterna magna.

2.3 Immunohistochemistry: Sample Preparation

At 1, 2, and 7 days following SAH or saline injection procedure for the time-matched control cohort, mice were perfusion fixed with 4% para-formaldehyde (PFA) (Sigma-Aldrich) (fig. 1). Cerebral tissue from all animals was dissected from the calvarium and post-fixed in 4% PFA for 5 hours. Following fixation, cerebral tissue was placed into 3% agarose (Type III-A, Sigma-Aldrich) and was sliced on a calibrated vibratome (Leica VT1000P) into 100 μm sections. Beginning at +1.10mm from Bregma, every fourth tissue section was collected until a total of eight sections had been acquired for tissue staining, and ultimately imaging.

2.4 Immunohistochemistry: Staining Protocol

The primary antibodies used were both diluted to 1:200 and included rat anti-mouse CD-68 (macrosialin, a marker of reactive macrophagic microglial cells) (MCA1957, Serotec) and rabbit anti-mouse CD-31 (PECAM-1, a marker of vascular endothelium) (ab28364, Abcam). The secondary antibodies used were both diluted to 1:250 and included donkey anti-rat Cy5 conjugated IgG (712-165-150, Jackson ImmunoResearch) and donkey anti-rabbit Cy3 conjugated IgG (711-166-152, Jackson ImmunoResearch). All sections were also treated with 0.05% 4′,6-diamidino-2-phenylindole (DAPI) (D-21490, Molecular Probes) as a nuclear stain. All sections were blocked with 0.5% Triton X-100 (Acros Organics) in 0.01M phosphate-buffered saline (PBS) (pH 7.4, Sigma-Aldrich) and 7% normal donkey serum (NDS) (017-000-121, Jackson ImmunoResearch). Primary and secondary agents were diluted in 0.1% Triton X-100/PBS and 1% NDS. Secondary antibodies alone served as negative controls. Antibodies were detected at the appropriate wavelength at a magnification of 40X on confocal microscopy (Olympus IX81, Fluoview v. 4.3), using a standard laser power, image PMT, and gain. In each of the eight slices collected, four evenly distributed 1024×1024 pixel images were obtained in each hemisphere at a uniform depth from the surface of the dorsal cortex. These regions of interest were objectively identified by initially selecting a field of view one field (1024 pixels, 317 μm) lateral of the central sulcus and one field (1024 pixels, 317 μm) deep of the dorsal cortical surface. Three additional regions of interest were then acquired, each separated by two fields of view and at a constant depth of one field from the dorsal cortical surface, in each cerebral hemisphere. All image acquisition was performed blinded to experimental group. Additionally, all subsequent image analysis was performed blinded to experimental group.

2.5 Image Analysis: Microglial Process Complexity

Using a novel proprietary program written in MatLab, microglial process complexity analysis was performed on automatically thresholded xyz image stacks (10–15 frames, 5 μm z-resolution) generated with confocal microscopy, which were then automatically converted to a binary pixel representation (1024 × 1024 pixels). Each image stack was analyzed on a frame-to-frame basis, not as a collapsed image to avoid inaccuracies. Microglia fluorescence (soma or process) was represented by white pixel, and background (gaps between cells) by black pixel. Scanning each pixel line horizontally from left to right, our program counted changes from black to white pixilation (Fig. 2A). Inactive microglia have highly branched, finer, and generally more complex processes in comparison to the less branched, thicker, simpler processes of activated microglia. Consequently, we expected to observe a greater number of black to white pixel transitions in quiescent microglia, and fewer black to white pixel transitions in activated microglia.

2.6 Image Analysis: Microglial Domain Volume

Using novel proprietary software, microglial domain volume analysis was performed on automatically thresholded xyz image stacks (10–15 frames, 5 μm z-resolution) generated with confocal microscopy, which were then automatically converted to a binary pixel representation (1024 × 1024 pixels) (Fig. 2B). A region of interest (ROI) surrounding a single microglia, and only this cell, was selected. Our program then calculated the surface area of this cell by measuring the area of white signal within the ROI. This step was then repeated for every frame the cell appeared in throughout a stack of images. The surface area for each frame was multiplied by the step size within the stack (5 μm) to arrive at an integrated volume of the cell. These integrated volumes were summed for an entire stack, to generate what we refer to as the microglial domain volume. This domain volume serves as an approximation of the true 3-dimentional microglial volume. This process was repeated for all microglia within the 1024×1024 pixel field of view where the top and bottom of the soma could be visualized. Microglia swell upon activation and take on a more amoeboid morphology, and while they retract processes, those processes remaining tend to be thicker; consequently, we expected that the absolute domain volume of these activated cells would be greater than their more ramified inactive counterparts (Fig. 2B).

2.7 Image Analysis: Microglial Distance to Nearest Capillary

Using ImageJ (http://rsbweb.nih.gov/ij/) the distances from all microglia nuclei (eGFP+/DAPI+) within a 500 × 500 pixel region of interest (ROI) centered within the greater 1024 × 1024 pixel field were measured to the nearest endothelial cell nucleus (CD-31+/DAPI+). Also, within the same ROI, the distances from the nuclei of activated (eGFP+/CD-68+/DAPI+) microglia to the nearest endothelial cell nucleus were measured.

2.8 Image Analysis: Microglial Cell Count

Using ImageJ the raw count of all microglia nuclei (eGFP+/DAPI+) within a 500 × 500 pixel ROI centered within the greater 1024 × 1024 pixel field were measured. Also, within the same ROI, the raw count of the activated microglia nuclei (eGFP+/CD-68+/DAPI+) was determined.

2.9 Statistical Analysis

Statistical analysis was performed with the aid of SigmaPlot 11.0 (Systat Software). The resulting values from microglial process complexity quantification, cell count, and distance to nearest capillary were evaluated using a one-way analysis of variance (ANOVA) with an all pair wise multiple comparison procedure (Holm-Sidak method). The following values from microglial domain volume quantification were evaluated using a one-way ANOVA with a multiple comparisons versus control group procedure (Holm-Sidak method). Probability values below 0.05 were deemed significant. All values are expressed as the mean +/− the standard error of the mean (SEM).

3. Results

3.1 Microglial Process Complexity Quantification

Using the previously outlined method of quantifying microglial process complexity (see 2.5) (fig. 2A) we were able to detect a statistically significant decrease in microglial process complexity 2 days following SAH when compared to controls (mean +/− SEM; 16438.077 +/− 909.986 vs. 21041.436 +/− 662.082, $p<0.05$) that then persists 7 days following the SAH incident (mean +/− SEM; 16799.211 +/− 1318.816 vs. 21041.436 +/− 662.082, $p<0.05$) (n = 4–6 animals per group) (fig. 3C).

3.2 Microglial Domain Volume Quantification

When we applied the prior discussed method of quantifying microglial domain volume (see 2.6) (fig. 2B), we observed a statistically significant increase in microglial domain volume 1 day following SAH when compared to controls (mean +/− SEM; 41606.396 +/− 6925.213 vs. 25644.716 +/− 1695.754, $p<0.05$); however, domain volume returned to baseline beginning 2 days after SAH, and this persisted at 7 days (n = 5–8 animals per group) (fig. 3D).

3.3 Microglial Distance to the Nearest Capillary

The literature has previously described the phenomenon of capillary failure in the post-SAH state (Dóczi, 2001; Friedrich et al., 2010; KoŸniewska et al., 2006; Perkins et al., 2002; Sehba and Friedrich, 2011; Sehba et al., 2005), and we have currently described that microglia demonstrate an activated morphology following SAH. Consequently, we attempted to determine if microglia change their position with respect to capillaries (identified by the vascular endothelial marker CD-31) as a possible mechanism of their failure, and if detection of this position change could also serve as a quantifiable metric of microglial activation over time. What is seen is that microglial position with respect to blood vessels, regardless of whether the cell is in an activated state or not, does not change 1, 2, or 7 days following SAH (n = 3–9 animals per group) (fig. 4A).

3.4 Microglial Cell Count

We next sought to determine if a known immunohistochemical method of detecting and quantifying microglial activation in other disease states (Peng et al., 2009) could be applied to SAH. Here we see that the raw count of microglia (eGFP+), as well as the subpopulation

that are activated (eGFP+/CD-68+), does not change 1, 2, or 7 days following SAH (n = 5–13 animals per group) (fig. 4B,C). The proportion of all microglia that are activated also does not change 1, 2, or 7 days following SAH (fig. 4D). Consequently, the quantifiable morphometric analysis of microglial activation that has been previously discussed, appears to be a more sensitive detection modality for appraising activation state and evaluating even small fluxes in this state over time when compared to spatiometric or even standard immunohistochemical methods.

4. Discussion

The present study is the first to describe a strong time-dependent activation of microglial morphology resulting from SAH insult using quantitative techniques that can be applied widely to the study of neuroinflammation after SAH. Most prior investigators have described qualitative microglial morphologic changes in various inflammatory and disease states (David and Kroner, 2011; Lawson et al., 1990; Zhang et al., 1997). These qualitative categorizations can be characterized as “ramified” at the inactive end of the spectrum, “bushy” at the active extreme, and “hypertrophied” absorbing all structures in between (Sotys et al., 2001). To this end we sought to develop novel image-processing techniques that would allow us to assign an objective, quantifiable measure to changes in morphology caused by SAH, and further, which would be sensitive enough in its assignment of these values to detect differences between active and inactive morphologies.

Previous work has similarly attempted to quantitatively assess the activation state of microglia in response to various injury and disease states. In our assessment, however, these prior studies have notable disadvantages to the techniques we presently describe. For example, Soltys *et al*. attempted to quantify microglial morphologic activation in lectin-stained cells (Soltys et al., 2005). Isoslectin I-B4 will bind alpha-D-galactosyl residues of polysaccharides and glycoproteins within the cell membrane, and thus will fail to label the entirety of the cell membrane and fine processes. As a result of this labeling technique, subtle changes in somatic size or shape, as well as process architecture, may go undetected. Here, a technique employing endogenous fluorescence, such as the use of the Cx3cr1-eGFP mouse, which will fill the entirety of the cytoplasm, represents an advancement improving the sensitivity of morphologic quantification.

Work by another group attempted to assess the activation state of microglia by imaging the ^{125}I-CLINDE radioligand, targeting the 18-kDa translocator protein (TSPO) (Arlicot et al., 2010). This technique relies on the fact that TSPO is minimally expressed in non-injured brain, where it is predominantly found in glial cells including both microglia and astrocytes (Benavides et al., 1983), but in various injury states, including stroke and neurodegeneration, its expression has been shown to increase in both of these cellular populations. As a result, this technique does not allow discernment between changes in TSPO expression attributable to astrocytes versus microglia, and thus there is no cell specificity in the evaluation of activation state with this method. Further, this technique only provides information on protein expression levels, without consideration of the more subtle differences in the reactive phenotype as microglia move along the spectrum from quiescent to active, which morphologic data would describe.

In an additional study by Kozlowski and colleagues, they used endogenously fluorescent microglia, as well as an automated technique for quantifying morphologic activation, similar to our study; however, here they only evaluated somatic morphology as an indicator of activation state (Kozlowski and Weimer, 2012). This only represents one aspect of morphologic activation, failing to address process complexity. As microglia use their processes to survey and respond to environmental stimuli, changes in process architecture should be directly evaluated in any study of morphologic reactivity. Further, the application of this technique of evaluating somatic size and shape to *in vivo*, two-photon microscopy, while showing promise towards the longitudinal evaluation of morphologic reactivity, may be prone of artifact due to the inflammatory process triggered by the craniotomy alone.

Similarly, recent work from our group applying a technique of microglial process complexity quantification to image stacks acquired through two-photon *in vivo* microscopy, may represent a deviation from normal physiology due to the necessity of imaging through a cranial window (Rangroo-Thrane et al., 2012). The present study's use of *ex vivo* imaging allows the freezing of the activation state in a more physiologic context. Further, when imaging very thin structures, such as individual cells and cellular processes, single photon (confocal) microscopes tend to demonstrate higher optical resolution due to their shorter excitation wavelengths. Thus, the application of this analytic technique to two-photon microscopy decreases the inherent sensitivity. Additionally, this study by Rangroo-Thrane *et al.* only examined process complexity and process turnover rate, whereas the current study sought to couple an analysis of process complexity with a metric of overall microglial volume to more sensitively and comprehensively understand the dynamics of microglial morphologic activation.

Lastly, there are commercially available morphology quantification products, such as that offered through Indica Labs Inc.; however, the highly proprietary nature of this software makes knowing the criteria for selecting active versus non-active microglia, as well as the methodology for identifying changes in various morphologic parameters, such as process complexity, ambiguous to the end user. This makes determining the accuracy and sensitivity of the assay in different histologic and imaging paradigms difficult. Further, the cost of obtaining this commercially available software puts it out of reach for many investigators.

Using propriety software written in MatLab we were able to develop two unique image-processing modalities, microglial process complexity and domain volume. We were able to detect a statistically significant decrease in microglial process complexity 2 days following SAH when compared to controls that then persisted 7 days following SAH. In addition, a statistically significant increase in microglial domain volume was observed 1 day following SAH when compared to controls; however, domain volume returned to baseline beginning 2 days after SAH. These findings demonstrate that our automated image processing techniques are sensitive enough to detect and quantitate changes in microglial morphology we would expect in response to injury; a decrease in the complexity of distal fine processes, and a swelling of the cell body and proximal processes. Beyond the automated nature of these analytic methods, which increases the convenience and efficiency of quantifying dynamic changes in cellular morphology, a further benefit of this analysis is the use of these tools in compliment with one another. Looking at each metric independently fails to

accurately capture the dynamic and complex nature of microglial activation across time. Most acutely microglial somata and processes transiently swell, while later process complexity declines and this effect appears to be more durable.

The development of these novel image analysis techniques will be vital to inform future studies which seek to establish quantitative thresholds for normal physiologic versus pathologic microglial morphologic activation in the spectrum of inflammatory responses. It would be interesting to compare the findings of the current study with those of another type of lesion known to induce microglial reactivity. For example, an ischemic insult or the injection of lipopolysaccharide would allow comparison of the time course of microglial reactivity seen in SAH, with attention to morphologic changes and expression of markers of activation. Assigning an objective measure to these immune cells' activation state will improve monitoring of disease progression as well as treatment response in the areas of both clinical and basic science medicine.

We must acknowledge that our mouse cisterna magna model of SAH may be limited in its ability to reproduce the pathophysiology of this disease chronically. In humans, vasospasm is thought to be an inflammatory reaction of the blood vessel wall developing between days 4 and 12 after SAH (Dumont et al., 2003; Sercombe et al., 2002; Suarez et al., 2006). In our mouse model, however, microglial morphologic activation, by definition also an inflammatory process, could not be detected beyond 7 days following SAH. As our model of SAH is a single autologous blood injection model, the volume of blood being delivered to the subarachnoid space is highly controlled and there are also no rebleeding episodes, and thus this model intrinsically lacks many of the defining characteristics of human SAH pathogenesis (Macdonald et al., 2007). Future studies will investigate the utility of a double injection model or an endovascular perforation model to study the delayed effects of SAH in mice (Sehba et al., 2007).

Having established both that microglia are activated morphologically following SAH, and that this activation can be quantified, we next sought to elucidate whether an immunohistochemical marker of microglial activation (CD-68, macrosialin) in other inflammatory settings (Peng et al., 2009) could be correlated with morphologic activation in the setting of SAH. What we found was that microglia, including the subpopulation that are CD-68+ and thus activated, do not increase in number following SAH. What this then means is that microgliosis following SAH does not involve resident proliferation of microglia or peripheral recruitment of monocytes (also express eGFP constitutively under Cx3cr1 promoter) across the blood brain barrier (Jung et al., 2000; Prinz and Priller, 2010). Additionally, it tends to suggest that CD-68 expression by microglia does not increase, and consequently the proportion of histologically active microglia does not rise following SAH. Immunohistochemical reactivity is highly dependent on the type of microglial reactivity present, and therefore an absence of detection of immunohistochemical activation does not necessarily mean there is no activation, as our morphometric analysis has revealed. While microglial activation is a progressive process, immunohistochemistry provides a very binary analysis of a cell's activation state: the cell either expresses a marker of activation or it does not. Our morphometric analysis looks beyond this "on vs. off" nature of activation and captures a spectrum of activation that is otherwise lost in other detection modalities. We

must again recognize, however, that due to the limitations of the current mouse cisterna magna model of SAH, we may not be reproducing the pathophysiology of this disease sufficiently and as a consequence the histologic inflammatory response may be subdued. Future work will focus on improving this model of SAH to better reflect the true disease state.

Our current findings suggest there is morphologic activation, both in process complexity and domain volume, of these immune effector cells following SAH. Additionally, it is known that the neurovascular unit is the interface between the circulation and the immune system (Dumont et al., 2003; Sercombe et al., 2002), and consequently we attempted to determine if activated microglia change their position with respect to capillaries following SAH. If detection of this position change could also serve as a quantifiable metric of microglial activation over time, then it could suggest that microglial activation reflects changes in microvascular function, immune activation, or both. Here, we see that there is no change in the distance distribution of microglia, both active and inactive, from the nearest capillary following SAH. This finding becomes informative when we consider the immune surveillance function of microglia (Bechmann et al., 2001; Ransohoff and Cardona, 2010). As we have been able to show, following SAH microglial activation takes the form of a decrease in process complexity, due to process retraction and loss of fimbriae, as well as an increase in domain volume, due to cellular hypertrophy. The combination of process retraction coupled together with a soma which does not change position with respect to surrounding capillaries, tends to suggest an impaired perivascular immune surveillance capability for microglia in the post-SAH inflammatory state. With impaired microglial surveillance of this perivascular space, and consequently decreased phagocytosis and clearance of pathogenic substances in the space, vascular inflammation may go unchecked leading ultimately to functional impairment of the microcirculation. While here we have only addressed the relationship between the circulation and microglia, an interesting application of our analytic techniques for future studies would be the evaluation of the relationship between neurons and reactive microglia cells and the impact this has on SAH progression and prognosis.

As this work was done *in situ*, a great limitation to this spatial analysis results from our ability to only measure distances in two-dimensions. Microglia distances from capillaries may be overestimated and their migration to positions more proximal to capillaries may be underestimated given a two-dimensional distance analysis where the third dimension of depth could not be taken into account in these calculations. Additionally, based on previous work from our group (Iliff et al., 2012), where fluorescently-labeled proteins and dextrans introduced to the CSF compartment via the cisterna magna were observed to move over the convexity of the dorsal cortex and down into the brain parenchyma via the paravascular spaces of penetrating arteries, we hypothesized that blood introduced to the basal cisterns via the cisterna magna would also travel up over the convexity of the dorsal cortical surface as the subarachnoid CSF carried it, and as a result all analyses throughout the present study strictly focused on the activation state of cortical microglia. While this is an inherent limitation of the current study, expanding the analysis to other brain regions will be an

important future step in determining if the described microglial morphologic activation is a more global effect occurring in deeper brain structures as well.

5. Conclusions

The activation of microglia revealed in this study illustrates the complex dynamics that interplay among morphology and the disease evolution of SAH. Using novel image analysis techniques we were able to describe a quantifiable activation of microglia following SAH, which may ultimately improve management of disease progression and response to anti-inflammatory treatments (Yenari et al., 2010; Yrjänheikki et al., 1998; Yrjänheikki et al., 1999).

Acknowledgments

7.1 Financial and Material Support:

This work was supported in part by NS057522 (GEV), NS 30007 and NS37073 (MN) from the US National Institutes of Health and the National Institute of Neurologic Disease and Stroke, by the Neurosurgery Research and Education Foundation of the American Association of Neurological Surgeons, by the Anspach Effort, and by the Brain Aneurysm Foundation.

Abbreviations

SAH	Subarachnoid hemorrhage
EBI	Early brain injury
eGFP	Enhanced green fluorescent protein
CX3CR1	Chemokine receptor 1 or fractalkine receptor
CD-68	Cluster of differentiation 68 or Macrosialin
CD-31	Cluster of differentiation 31 or platelet endothelial cell adhesion molecule 1 or PECAM-1
ROI	Region of interest
DAPI	4′,6-diamidino-2-phenylindole
SEM	Standard error of the mean

References

Arlicot N, Petit E, Katsifis A, Toutain J, Divoux D, Bodard S, Roussel S, Guilloteau D, Bernaudin M, Chalon S. Detection and quantification of remote microglial activation in rodent models of focal ischaemia using the TSPO radioligand CLINDE. European Journal of Nuclear Medicine and Molecular Imaging. 2010; 37:2371–80. [PubMed: 20814674]

Bechmann I, Priller J, Kovac A, Böntert M, Wehner T, Klett FF, Bohsung J, Stuschke M, Dirnagl U, Nitsch R. Immune surveillance of mouse brain perivascular spaces by blood-borne macrophages. The European Journal of Neuroscience. 2001; 14:1651–8. [PubMed: 11860459]

Benavides J, Quarteronet D, Imbault F, Malgouris C, Uzan A, Renault C, et al. Labelling of “peripheral-type” benzodiazepine binding sites in the rat brain by using [3H]PK 11195, an isoquinoline carboxamide derivative: kinetic studies and autoradiographic localization. Journal of Neurochemistry. 1983; 41:1744–50. [PubMed: 6315880]

Cahill J, Zhang JH. Subarachnoid hemorrhage: is it time for a new direction? Stroke; a Journal of Cerebral Circulation. 2009; 40:S86–7-S-7.

Crowley RW, Medel R, Dumont AS, Ilodigwe D, Kassell NF, Mayer SA, Ruefenacht D, Schmiedek P, Weidauer S, Pasqualin A, Macdonald RL. Angiographic Vasospasm Is Strongly Correlated With Cerebral Infarction After Subarachnoid Hemorrhage. Stroke; a Journal of Cerebral Circulation. 2011

David S, Kroner A. Repertoire of microglial and macrophage responses after spinal cord injury. Nature Reviews. Neuroscience. 2011

Dóczi TP. Impact of cerebral microcirculatory changes on cerebral blood flow during cerebral vasospasm after aneurysmal subarachnoid hemorrhage. Stroke; a Journal of Cerebral Circulation. 2001; 32:817.

Dreier JP. The role of spreading depression, spreading depolarization and spreading ischemia in neurological disease. Nature Medicine. 2011; 17:439–47.

Dreier JP, Ebert N, Priller J, Megow D, Lindauer U, Klee R, Reuter U, Imai Y, Einhäupl KM, Victorov I, Dirnagl U. Products of hemolysis in the subarachnoid space inducing spreading ischemia in the cortex and focal necrosis in rats: a model for delayed ischemic neurological deficits after subarachnoid hemorrhage? Journal of Neurosurgery. 2000; 93:658–66. [PubMed: 11014545]

Dreier JP, Woitzik J, Fabricius M, Bhatia R, Major S, Drenckhahn C, Lehmann T-N, Sarrafzadeh A, Willumsen L, Hartings JA, Sakowitz OW, Seemann JH, Thieme A, Lauritzen M, Strong AJ. Delayed ischaemic neurological deficits after subarachnoid haemorrhage are associated with clusters of spreading depolarizations. Brain: A Journal of Neurology. 2006; 129:3224–37. [PubMed: 17067993]

Dumont AS, Dumont RJ, Chow MM, Lin C-L, Calisaneller T, Ley KF, Kassell NF, Lee KS. Cerebral vasospasm after subarachnoid hemorrhage: putative role of inflammation. Neurosurgery. 2003; 53:123–33. discussion 33-35--33; discussion 33–35. [PubMed: 12823881]

Friedrich V, Flores R, Muller A, Sehba FA. Luminal platelet aggregates in functional deficits in parenchymal vessels after subarachnoid hemorrhage. Brain Research. 2010; 1354:179–87. [PubMed: 20654597]

Frijns CJM, Kappelle LJ. Inflammatory cell adhesion molecules in ischemic cerebrovascular disease. Stroke; a Journal of Cerebral Circulation. 2002; 33:2115–22.

Graeber MB. Changing face of microglia. Science (New York, NY). 2010; 330:783–8.

Hansen-Schwartz J, Vajkoczy P, Macdonald RL, Pluta RM, Zhang JH. Cerebral vasospasm: looking beyond vasoconstriction. Trends in Pharmacological Sciences. 2007; 28:252–6. [PubMed: 17466386]

Iliff JJ, Wang M, Liao Y, Plog BA, Peng W, Gundersan GA, Benveniste H, Vates GE, Deane R, Goldman SA, Nagelhus EA, Nedergaard M. A paravascular pathway facilitates CSF flow through the brain parenchyma and the clearance of interstitial soluted, including amyloid β. Science Translational Medicine. 2012; 4:1–11.

Jung S, Aliberti J, Graemmel P, Sunshine MJ, Kreutzberg GW, Sher A, Littman DR. Analysis of fractalkine receptor CX(3)CR1 function by targeted deletion and green fluorescent protein reporter gene insertion. Molecular and Cellular Biology. 2000; 20:4106–14. [PubMed: 10805752]

Kozlowski C, Weimer RM. An automated method to quantify microglia morphology and application to monitor activation state longitudinally in vivo. PLoS ONE. 2012; 7:1–9.

KoŸniewska E, Michalik R, Rafałowska J, Gadamski R, Walski M, Frontczak-Baniewicz M, Piotrowski P, Czernicki Z. Mechanisms of vascular dysfunction after subarachnoid hemorrhage. Journal of Physiology and Pharmacology: An Official Journal of the Polish Physiological Society. 2006; 57 (Suppl 11):145–60.

Lawson LJ, Perry VH, Dri P, Gordon S. Heterogeneity in the distribution and morphology of microglia in the normal adult mouse brain. Neuroscience. 1990; 39:151–70. [PubMed: 2089275]

Liu W, Tang Y, Feng J. Cross talk between activation of microglia and astrocytes in pathological conditions in the central nervous system. Life Sciences. 2011

Macdonald RL, Pluta RM, Zhang JH. Cerebral vasospasm after subarachnoid hemorrhage: the emerging revolution. Nature Clinical Practice Neurology. 2007; 3:256–63.

Murakami K, Koide M, Dumont TM, Russell SR, Tranmer BI, Wellman GC. Subarachnoid Hemorrhage Induces Gliosis and Increased Expression of the Pro-inflammatory Cytokine High Mobility Group Box 1 Protein. Translational Stroke Research. 2011; 2:72–9. [PubMed: 21479116]

Ostrowski RP, Colohan AR, Zhang JH. Molecular mechanisms of early brain injury after subarachnoid hemorrhage. Neurological Research. 2006; 28:399–414. [PubMed: 16759443]

Peng W, Cotrina ML, Han X, Yu H, Bekar L, Blum L, Takano T, Tian G-F, Goldman SA, Nedergaard M. Systemic administration of an antagonist of the ATP-sensitive receptor P2X7 improves recovery after spinal cord injury. Proceedings of the National Academy of Sciences. 2009; 106:12489–93.

Perkins E, Kimura H, Parent AD, Zhang JH. Evaluation of the microvasculature and cerebral ischemia after experimental subarachnoid hemorrhage in dogs. Journal of Neurosurgery. 2002; 97:896–904. [PubMed: 12405379]

Pluta RM, Hansen-Schwartz J, Dreier J, Vajkoczy P, Macdonald RL, Nishizawa S, Kasuya H, Wellman G, Keller E, Zauner A, Dorsch N, Clark J, Ono S, Kiris T, Leroux P, Zhang JH. Cerebral vasospasm following subarachnoid hemorrhage: time for a new world of thought. Neurological Research. 2009; 31:151–8. [PubMed: 19298755]

Prinz M, Priller J. Tickets to the brain: role of CCR2 and CX3CR1 in myeloid cell entry in the CNS. Journal of Neuroimmunology. 2010; 224:80–4. [PubMed: 20554025]

Rangroo-Thrane V, Thrane AS, Chanag J, Alleluia V, Nagelhus EA, Nedergaard M. Real-time analysis of microglial activation and motility in hepatic and hyperammonemic encephalopathy. Neuroscience. 2012; 220:247–55. [PubMed: 22728097]

Ransohoff RM, Cardona AE. The myeloid cells of the central nervous system parenchyma. Nature. 2010; 468:253–62. [PubMed: 21068834]

Rosengart AJ, Schultheiss KE, Tolentino J, Macdonald RL. Prognostic factors for outcome in patients with aneurysmal subarachnoid hemorrhage. Stroke; a Journal of Cerebral Circulation. 2007; 38:2315–21.

Sehba FA, Bederson JB. Mechanisms of acute brain injury after subarachnoid hemorrhage. Neurological Research. 2006; 28:381–98. [PubMed: 16759442]

Sehba FA, Friedrich V. Early micro vascular changes after subarachnoid hemorrhage. Acta Neurochirurgica Supplement. 2011; 110:49–55. [PubMed: 21116914]

Sehba FA, Friedrich V Jr, Makonnen G, Bederson JB. Acute cerebral vascular injury after subarachnoid hemorrhage and its prevention by administration of a nitric oxide donor. Journal of Neurosurgery. 2007; 106:321–9. [PubMed: 17410718]

Sehba FA, Mostafa G, Friedrich V Jr, Bederson JB. Acute microvascular platelet aggregation after subarachnoid hemorrhage. Journal of Neurosurgery. 2005; 102:1094–100. [PubMed: 16028769]

Sehba FA, Mostafa G, Knopman J, Friedrich V Jr, Bederson JB. Acute alterations in microvascular basal lamina after subarachnoid hemorrhage. Journal of Neurosurgery. 2004; 101:633–40. [PubMed: 15481718]

Sehba FA, Pluta RM, Zhang JH. Metamorphosis of subarachnoid hemorrhage research: from delayed vasospasm to early brain injury. Molecular Neurobiology. 2011; 43:27–40. [PubMed: 21161614]

Sercombe R, Dinh YRT, Gomis P. Cerebrovascular inflammation following subarachnoid hemorrhage. Japanese Journal of Pharmacology. 2002; 88:227–49. [PubMed: 11949877]

Simi A, Tsakiri N, Wang P, Rothwell NJ. Interleukin-1 and inflammatory neurodegeneration. Biochemical Society Transactions. 2007; 35:1122–6. [PubMed: 17956293]

Soltys Z, Orzylowska-Sliwinska O, Zaremba M, Orlowski D, Piechota M, Fiedorowicz A, Janeczko K, Oderfeld-Nowak B. Quantitative morphological study of microglial cells in the ischemic rat brain using principal componenet analysis. Journal of Neuroscience Methods. 2005; 146:50–60. [PubMed: 15935220]

Sotys Z, Ziaja M, Pawliski R, Setkowicz Z, Janeczko K. Morphology of reactive microglia in the injured cerebral cortex. Fractal analysis and complementary quantitative methods. Journal of Neuroscience Research. 2001; 63:90–7. [PubMed: 11169618]

Suarez JI, Tarr RW, Selman WR. Aneurysmal subarachnoid hemorrhage. The New England Journal of Medicine. 2006; 354:387–96. [PubMed: 16436770]

Vergouwen MDI, Ilodigwe D, Macdonald RL. Cerebral Infarction After Subarachnoid Hemorrhage Contributes to Poor Outcome by Vasospasm-Dependent and -Independent Effects. Stroke; a Journal of Cerebral Circulation. 2011

Yenari MA, Kauppinen TM, Swanson RA. Microglial activation in stroke: therapeutic targets. Neurotherapeutics: The Journal of the American Society for Experimental NeuroTherapeutics. 2010; 7:378–91. [PubMed: 20880502]

Yrjänheikki J, Keinänen R, Pellikka M, Hökfelt T, Koistinaho J. Tetracyclines inhibit microglial activation and are neuroprotective in global brain ischemia. Proceedings of the National Academy of Sciences of the United States of America. 1998; 95:15769–74. [PubMed: 9861045]

Yrjänheikki J, Tikka T, Keinänen R, Goldsteins G, Chan PH, Koistinaho J. A tetracycline derivative, minocycline, reduces inflammation and protects against focal cerebral ischemia with a wide therapeutic window. Proceedings of the National Academy of Sciences of the United States of America. 1999; 96:13496–500. [PubMed: 10557349]

Zhang Z, Chopp M, Powers C. Temporal profile of microglial response following transient (2 h) middle cerebral artery occlusion. Brain Research. 1997; 744:189–98. [PubMed: 9027378]

Highlights

- Development of a novel morphometric analysis to quantify microglia activation following SAH.
- This analysis revealed a decrease in microglial process complexity 2 and 7 days following SAH.
- Further, this analysis demonstrated an increase in microglial domain volume 1 day following SAH.
- This work represents advancement in glial cell morphometric quantification capabilities.
- These tools increase understanding of the time course and degree of microglia activation after SAH.

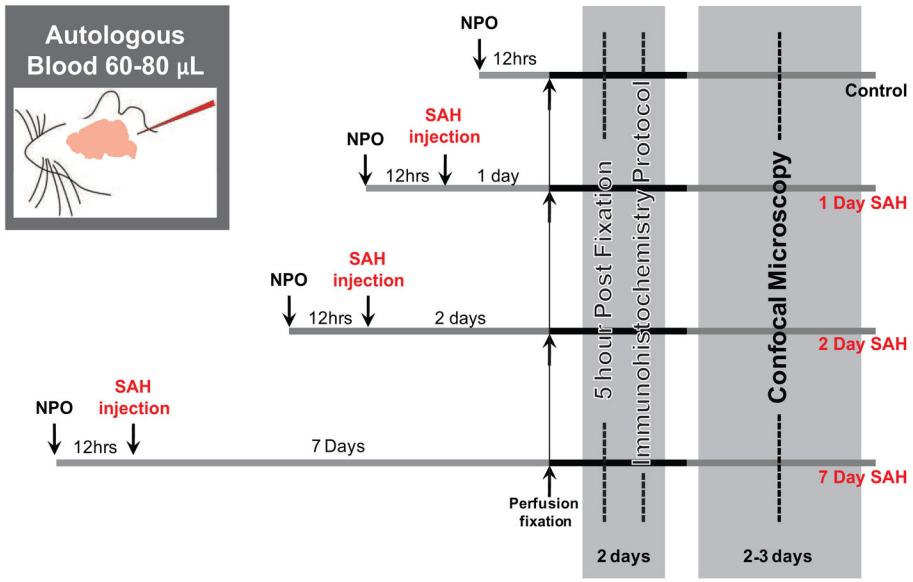

Figure 1.

Experimental timeline. Mice were randomly assigned to one of four experimental conditions: control, 1 day SAH, 2 day SAH and 7 day SAH (top to bottom, respectively). Inset illustrates cisterna magna injection of autologous blood in our mouse model of SAH.

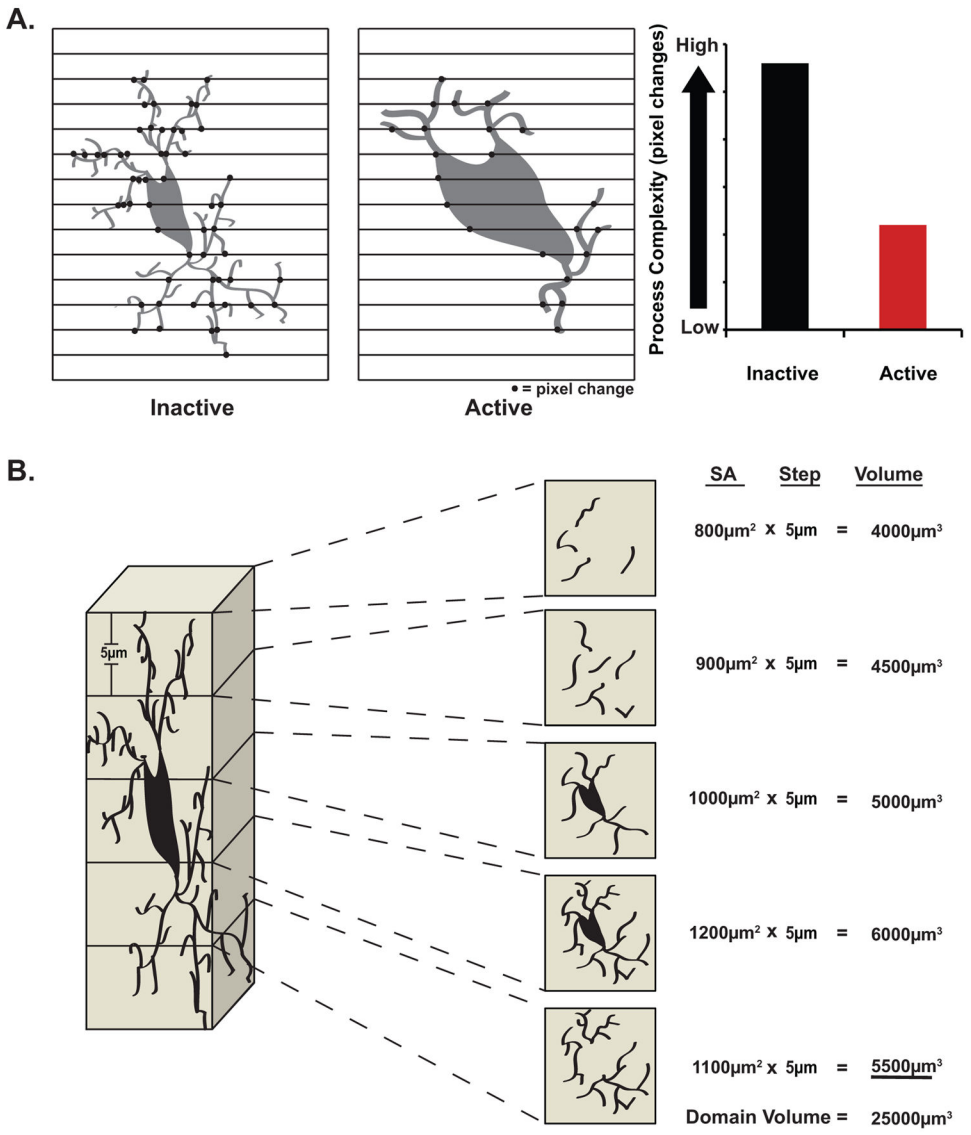

Figure 2.

Novel morphometric quantification of microglial activation. Using propriety software written in MatLab we were able to develop two unique methods of both detecting and quantifying the degree of microglial activation following SAH. **A.** Diagrammatic representation of process complexity analysis demonstrating greater black to white pixilation changes with inactive versus active microglia. **B.** Diagrammatic representation of domain volume analysis for a single microglia through its entire depth. (See *sections 2.5 and 2.6* for greater description of these two methods of morphologic quantification).

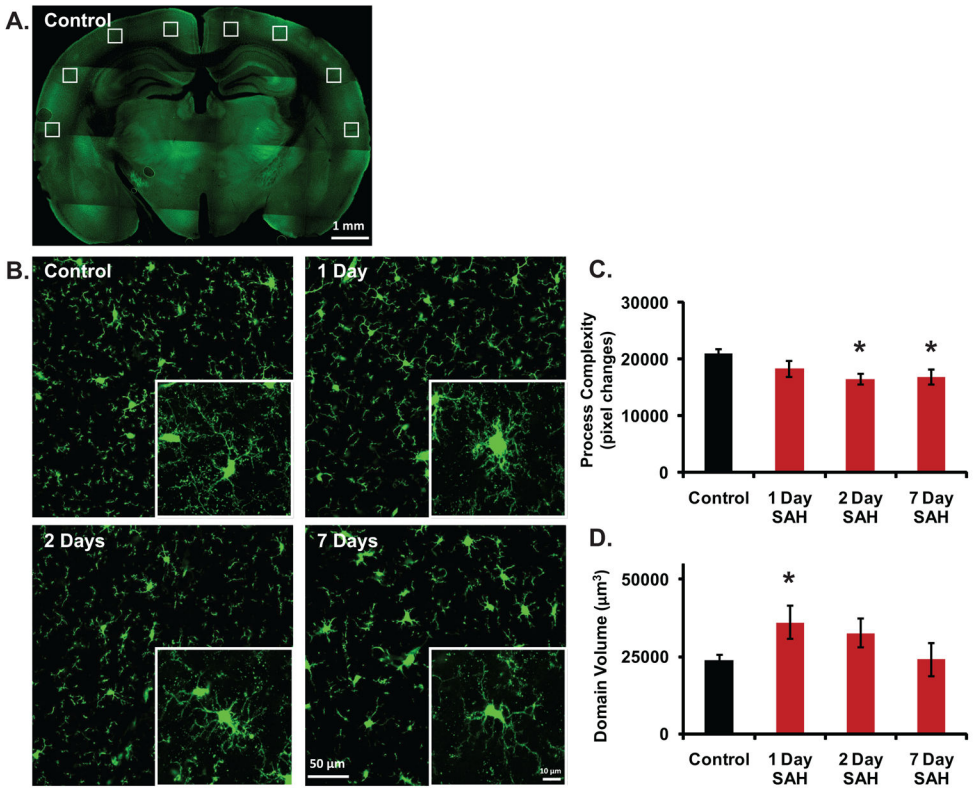

Figure 3.

Novel image-processing techniques can sensitively assay for morphologic activation of microglia and quantify this activation along a spectrum of inflammatory responses. **A.** Low magnification (4X) montage image of control Cx3cr1-eGFP brain slice demonstrating standardized location of image acquisition within bilateral cerebral cortices. **B.** Representative high magnification (40X) images used for quantification of microglial morphology under control conditions and 1, 2, and 7 days following SAH. Insets are representative 100X images demonstrating detailed changes in single cell architecture under control conditions and 1, 2, and 7 days following SAH. **C.** A statistically significant decrease in microglial process complexity was observed 2 days following SAH when compared to controls (mean +/− SEM; 16438.077 +/− 909.986 vs. 21041.436 +/− 662.082, $p<0.05$) that persisted 7 days following SAH (mean +/− SEM; 16799.211 +/− 1318.816 vs. 21041.436 +/− 662.082, $p<0.05$) (n = 4–6 animals per group). **D.** A statistically significant increase in microglial domain volume was observed 1 day following SAH when compared to controls (mean +/− SEM; 41606.396 +/− 6925.213 vs. 25644.716 +/− 1695.754); however, we observed domain volume returned to baseline beginning 2 days after SAH (n = 5–8 animals per group). *Key:* green signal = eGFP. All bars graphs represent mean +/− SEM; * $p<0.05$.

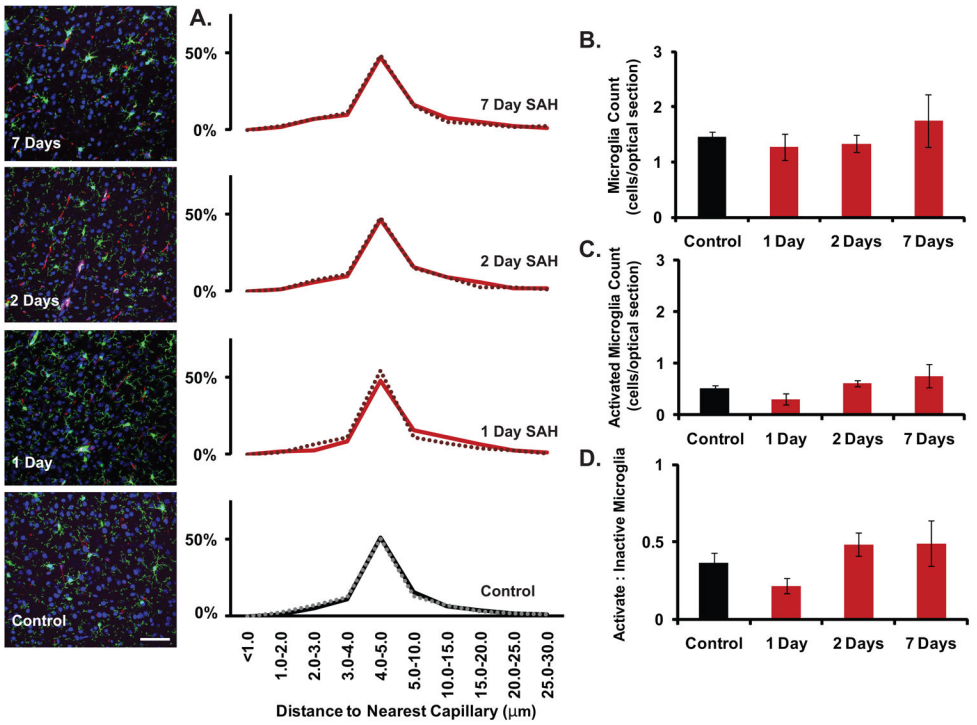

Figure 4.

No change in microglial position with respect to the nearest capillary, or in expression of the histochemical activation marker CD-68 could be detected. **A.** Microglial position with respect to the nearest capillary, regardless of whether the cell is activated or not, did not change 1, 2, or 7 days following SAH (n = 3–9 animals per group). **B., C.** The raw count of microglia, as well as the subpopulation which are eGFP+/CD-68+ and thus activated, did not change 1, 2, or 7 days following SAH (n = 5–13 animals per group). **D.** The proportion of all microglia that are activated also did not change 1, 2, or 7 days following SAH (n = 5–13 animals per group). *Key:* green signal = eGFP, red signal = CD-31, magenta signal = CD-68, and blue signal = DAPI. All bars graphs represent mean +/− SEM.